Laser-induced 3D alignment and orientation of quantum-state-selected molecules

Iftach Nevo[1], Lotte Holmegaard[1], Jens H. Nielsen[2], Jonas L. Hansen[3], and Henrik Stapelfeldt[1,3*]
[1] *Department of Chemistry, University of Aarhus, DK-8000 Aarhus C, Denmark*
[2] *Department of Physics and Astronomy, University of Aarhus, DK-8000 Aarhus C, Denmark*
[3] *Interdisciplinary Nanoscience Center (iNANO), University of Aarhus, DK-8000 Aarhus C, Denmark*

Frank Filsinger, Gerard Meijer, and Jochen Küpper[†]
Fritz-Haber-Institut der Max-Planck-Gesellschaft, Faradayweg 4-6, 14195 Berlin, Germany
(Dated: June 10, 2013)

A strong inhomogeneous static electric field is used to spatially disperse a rotationally cold supersonic beam of 2,6-difluoroiodobenzene molecules according to their rotational quantum state. The molecules in the lowest lying rotational states are selected and used as targets for 3-dimensional alignment and orientation. The alignment is induced in the adiabatic regime with an elliptically polarized, intense laser pulse and the orientation is induced by the combined action of the laser pulse and a weak static electric field. We show that the degree of 3-dimensional alignment and orientation is strongly enhanced when rotationally state-selected molecules, rather than molecules in the original molecular beam, are used as targets.

PACS numbers: 36.80.-i,36.40.Wa

I. INTRODUCTION

The spatial orientation of a molecule is of crucial importance for its interactions with other molecules, atoms, or electromagnetic radiation. Driven by the possibility of controlling or enhancing molecular reactivity and interactions [1–3], as well as by possibilities for new research directions in molecular science, including imaging of molecular orbitals [4] and photoelectron angular distribution from fixed-in-space molecules [5, 6], large efforts have been devoted to developing methods that enable control over the orientation or alignment of molecules. Here, alignment refers to confinement of molecule-fixed axes along laboratory-fixed axes, and orientation refers to the molecular dipole moments pointing in a particular direction.

In the gas phase, the electric fields from moderately intense, nonresonant laser pulses have proven particularly useful and versatile for manipulating the alignment of molecules [7]. A laser field induces an electric dipole moment in any molecule with a polarizability anisotropy, whether polar or not, and the interaction between the induced dipole and the laser field itself forces the molecule to align. In the case of a linearly polarized laser field the most polarizable axis is aligned along the polarization direction, which is sufficient to ensure strong angular confinement of the figure axis of the molecules and, therefore, complete alignment control of linear and symmetric top molecules. This is termed 1-dimensional (1D) alignment. For asymmetric top molecules 1D alignment does not suffice to provide complete alignment control. Rather, all three molecular axes of polarisability must be confined to laboratory fixed axes. Such 3-dimensional (3D) alignment has been experimentally demonstrated through the use of an elliptically polarized laser field [8–11] or by combining two linearly polarized laser pulses with orthogonal polarizations [12–15].

In the case of polar molecules confinement of the molecular axes is not sufficient to achieve full orientational control; it is also necessary to control the direction of the permanent dipole. As suggested by Friedrich and Herschbach a decade ago [16, 17], and later demonstrated experimentally [10, 18–21], orientation can be added to alignment by combining the strong laser field with a weak static electric field. Therefore, we use 1D orientation to denote 1D alignment and, simultaneously, a preferred direction of the permanent dipole moment. Likewise, 3D orientation refers to 3D alignment occurring together with a preferred direction of the permanent dipole moment.

Any application of aligned or oriented molecules will benefit significantly, or simply require, that the degree of alignment or orientation is strong. One efficient method to optimize the degree of alignment or orientation is to ensure that the molecular sample initially resides in the lowest lying rotational states. This is achieved by lowering the rotational temperature as much as possible. In practice, strong cooling can be obtained by supersonically expanding a small fraction of the molecular gas of interest in an inert carrier gas. Very strong degrees of alignment have been reported using molecular beams with a rotational temperature around 1 K [22]. Optimizing the degree of orientation in the mixed laser and static electric field method imposes, however, an even stronger requirement on the initial rotational state distribution. Recently, we showed that 1D orientation, using the mixed-field method, can be strongly enhanced by using rotational-quantum-state selected molecules as targets [21, 23]. The state selection is obtained by passing

*Electronic address: henriks@chem.au.dk
†Electronic address: jochen@fhi-berlin.mpg.de

a cold molecular beam through an electrostatic deflector that spatially disperses molecules according to their rotational quantum state. The purpose of the present work is to demonstrate that the use of rotational-state-selected molecules also enables significant improvement of laser induced 3D alignment and mixed-field 3D orientation.

The studies are carried out on 2,6-difluoroiodobenzene (DFIB) molecules in the adiabatic limit, where the alignment laser pulse is turned on and off slowly compared to the inherent rotational periods of the molecules [7]. In this regime the degree of alignment and orientation will follow the envelope of the 10-ns-long applied laser pulse. In particular, the strongest degree of alignment occurs at the peak of the pulse, which is the point in time where all measurements in this work are recorded. From quantum-chemistry calculations at the B3LYP [24, 25]/TZVPP [26] level using linear response theory in the Turbomole 5.10 program suite [27], the polarizability components of the DFIB molecules are determined to be α_{zz} = 21.3 Å^3, α_{yy} = 14.5 Å^3, and α_{xx} = 8.5 Å^3, where the z-axis is parallel to the C-I axis, the y-axis is perpendicular to the z-axis but still in the molecular plane, and the x-axis is perpendicular to the molecular plane. It is therefore expected that a linearly polarized laser field will align the C-I axis along the polarization axis. With an elliptically polarized beam the largest polarizability axis of the molecule is expected to be aligned along the major axis of the elliptical field and the second most polarizable axis along the minor axis of the field. Therefore, it is expected that an elliptically polarized field will align the C-I axis along the major polarization axis and the molecular plane to the polarization plane. The case of such 1D and 3D alignment is discussed in Section III B and the alignment enhancement employing state-selected molecules is demonstrated. The permanent electric dipole moment of DFIB is 2.25 D. It is parallel to the C-I axis with the negative end pointing in the direction of the iodine atom. Consequently, it is expected that a static electric field, collinear with the major polarization axis of the alignment field, will force the iodine end of each molecule to point in the direction of the positive electrode of the static field. The case of 1D and 3D orientation and the advantage of using state selected molecules is discussed in Section III C.

II. EXPERIMENTAL SETUP

A schematic of the experimental setup, which is described in detail elsewhere [23], is shown in Figure 1. A mixture of a few mbar of DFIB and 90 bar of helium is expanded into vacuum using a pulsed Even-Lavie valve [28] to produce a molecular beam with a rotational temperature of approximately 1 K. After passing two 1-mm-diameter skimmers the molecular beam enters a 15-cm-long electrostatic beam deflector. The deflector consists of a trough (at ground potential) with an inner

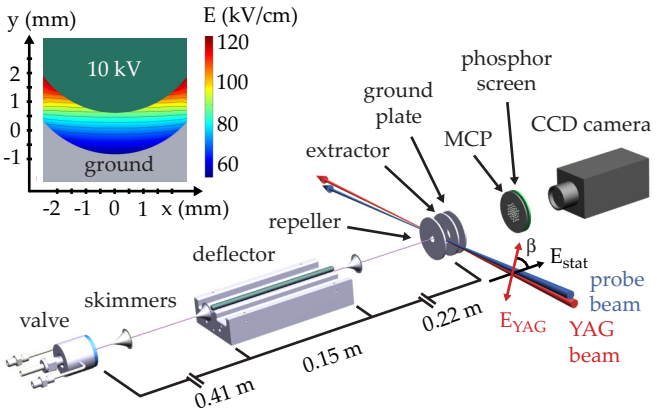

FIG. 1: (Color online) Scheme of the experimental setup. In the inset, a cut through the deflector is shown and a contour-plot of the electric field strength is given. $\beta = 0$ corresponds to the case of the major axis of laser polarization oriented along the TOF axis.

radius of curvature of 3.2 mm and a rod (at high voltage) with a radius of 3.0 mm. The vertical separation of the two electrodes across the molecular beam axis is 1.4 mm. This electrode geometry creates a two-wire field with a nearly constant gradient over a large area around the molecular beam axis [29]. In the inset of Figure 1, a cross sectional view of the deflector with the created electric field is given. The deflector is mounted such that the deflection occurs vertically, and molecules in high-field-seeking states are deflected upwards.

After passing the deflector, the molecular beam enters the target/detection area through a 1.5-mm-diameter skimmer where it is crossed by one or two laser beams that are focused by a spherical lens with a focal length of f = 300 mm. The lens is mounted on a vertical translation stage so that the height of the laser foci can be adjusted with high precision. One laser beam, consisting of 30-fs-long pulses (800 nm, beam-waist of ω_0 = 21 μm which corresponds to 4×10^{14} W/cm^2) is used to probe the molecules. In the first part of the experiment, this laser beam is used to characterize the deflection by determining the density, at a given height, of the molecular beam via photoionization. Hereafter, this laser beam is used for Coulomb exploding the molecules to determine their alignment and orientation by imaging the ionized fragments on the plane of the microchannel plate (MCP) detector. The second laser beam, consisting of 10-ns-long pulses from a Nd:YAG laser (1064 nm, ω_0 = 36 μm), is used to align and orient the molecules. Two intensity values of the pulses were applied: 1.2×10^{12} and 1.8×10^{11} W/cm^2, denoted hereafter as $I_{YAG,high}$ and $I_{YAG,low}$, respectively.

The probe pulse is electronically synchronized to the peak of the YAG pulse. Positive ions produced by the probe pulses are accelerated, in a velocity focusing geometry, towards a MCP detector backed by a phosphor screen. The 2D ion images are recorded with a CCD

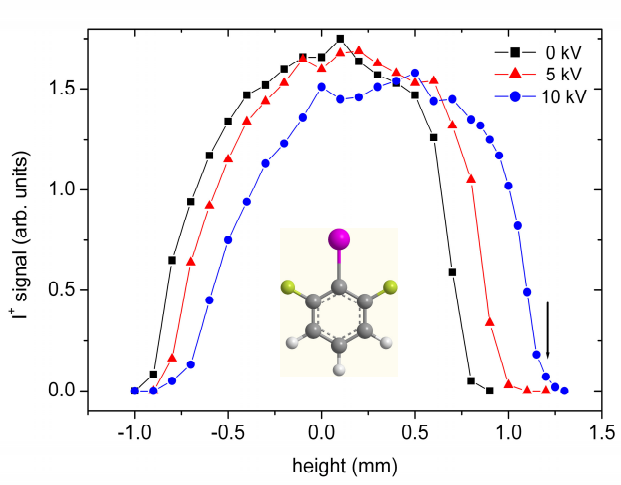

FIG. 2: (Color online) Vertical profiles of the molecular beam measured by recording the I^+ signal as a function of the vertical position of the fs probe beam focus. The experimental data are shown by black squares (deflector off, 0 kV), red triangles (5 kV), and blue circles (10 kV). The arrow denotes the position of the probe laser focus for acquiring images and TOF spectra of deflected molecules. A model of the DFIB molecule is shown as an inset.

camera. In particular, the I^+ and F^+ fragment ion distributions are useful experimental observables since these ions recoil along the symmetry axis and in the plane of the molecule, respectively. Thereby, they allow the determination of the molecular orientation at the time of the probe pulse. Also, the time-of-flight (TOF) of the ions from the laser-interaction spot to the MCP is recorded. The experiments are conducted at 20 Hz, limited by the repetition rate of the YAG laser.

III. RESULTS AND DISCUSSIONS

A. Deflection of the molecular beam

The effect of the deflector on the molecular beam is illustrated in Figure 2 by the vertical intensity profiles, which are obtained by recording the I^+ signal from photoionization due to the femtosecond probe laser as a function of the vertical position of the laser focus. When the deflector is turned off, the molecular beam extends over ~ 1.7 mm, mainly determined by the diameter of the last skimmer before the target area. When the deflector is turned on, the molecular beam profile shifts upwards (by 0.4 mm at 10 kV). The shift becomes more pronounced as the voltage on the deflector is increased from 5 kV to 10 kV. Molecules in the lowest rotational quantum states have the largest Stark shifts and are, therefore, deflected the most, as shown in our recent work on iodobenzene molecules [21, 23]. In the measurements described below, experiments have been conducted on these quantum-state selected molecules simply by positioning the laser foci close to the upper cut-off region in the 10 kV profile, as indicated by the arrow in Figure 2 (*height* = 1.2 *mm*).

B. 1-dimensional and 3-dimensional alignment

We start by showing that a linearly polarized YAG pulse induces 1D alignment of the DFIB molecules. We compare I^+ images recorded with and without the YAG pulse when the deflector is turned off. In the absence of the YAG pulse, the I^+ image is circularly symmetric (Figure 3 A) due to the circular symmetry introduced by polarizing the probe pulse perpendicular to the detector plane. When the YAG pulse, polarized parallel to the detector plane, is applied, the I^+ ions exhibit strong angular localization about the polarization axis, as depicted in Figure 3 B, showing that the C-I axis of the molecules is strongly confined along the YAG polarization, i. e., the DFIB molecules are 1D adiabatically aligned. Consequently, images taken with the YAG polarization in the detector plane can be regarded as a "side-view" of the molecule. The degree of alignment is quantified by $\langle\cos^2\theta_{2D}\rangle = 0.94$, where θ_{2D} is the angle between the projection of the I^+ recoil velocity on the detector plane and the YAG polarization [22]. The I^+ ions appear as two sets of angularly narrow rings. The innermost (and brightest) ring results from I^+ ions when DFIB is doubly ionized by the probe pulse and fragments into an $I^+ + C_6H_3F_2^+$ ion pair, whereas the outermost ring results from I^+ ions formed from triple ionization and fragmentation into an $I^+ + C_6H_3F_2^{2+}$ ion pair [30]. The value of $\langle\cos^2\theta_{2D}\rangle$ is determined in the radial range corresponding to the outermost ring. By comparison, in the absence of the YAG pulse $\langle\cos^2\theta_{2D}\rangle = 0.50$, as expected for randomly oriented molecules. When the deflector is turned on and the laser foci moved close to the upper cutoff region in the 10 kV profile (*height* = 1.2 mm), corresponding to the lowest lying rotational states of the DFIB molecules, the 1D alignment sharpens. This is evident by comparing Figure 3 B and D and noting that $\langle\cos^2\theta_{2D}\rangle$ increases to 0.96. The improved alignment is consistent with our recent experiments on iodobenzene [21, 23].

Similarly, images taken with the YAG pulse polarized perpendicular to the detector plane show "end-views" of the molecules. All images in Figure 4 are recorded in the end-view. The tight confinement of the I^+ ions near the center (A2–A4 and C2–C4), compared to the I^+ distribution without the YAG pulse (Figure 4 A1 and C1) is an alternative way to visualize the 1D alignment. In order to quantify the angular confinement, the average distances $\langle X\rangle$ and $\langle Y\rangle$ of I^+ ions along the horizontal (X) and vertical axes (Y) from the center of the end-view images are calculated, see Figure 4 (A1). Without the YAG $\langle X\rangle = 37.4$ pixels and $\langle Y\rangle = 34.8$ pixels. Including the YAG $\langle X\rangle = 19.0$ pixels and $\langle Y\rangle = 19.0$ pixels without voltages applied to the deflector (Image A2 in Figure 4), and $\langle X\rangle = 12.3$ pixels and $\langle Y\rangle = 12.2$ pixels with 10 kV

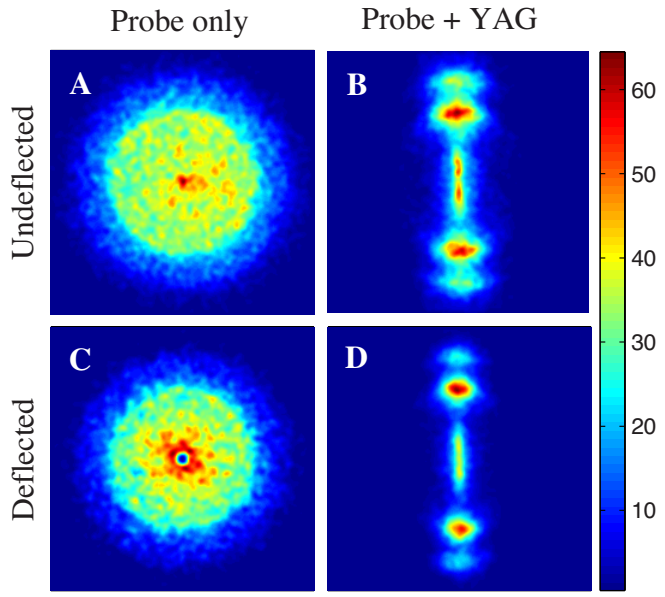

FIG. 3: (Color online) Alignment of DFIB molecules induced by a linearly polarized YAG pulse, illustrated by velocity map images of the I^+ ions. A, C: I^+ images recorded without the YAG pulse for undeflected and deflected, respectively. B, D: I^+ images with the YAG included (vertical polarization, $I_{YAG,high}$) using undeflected and deflected molecules, respectively.

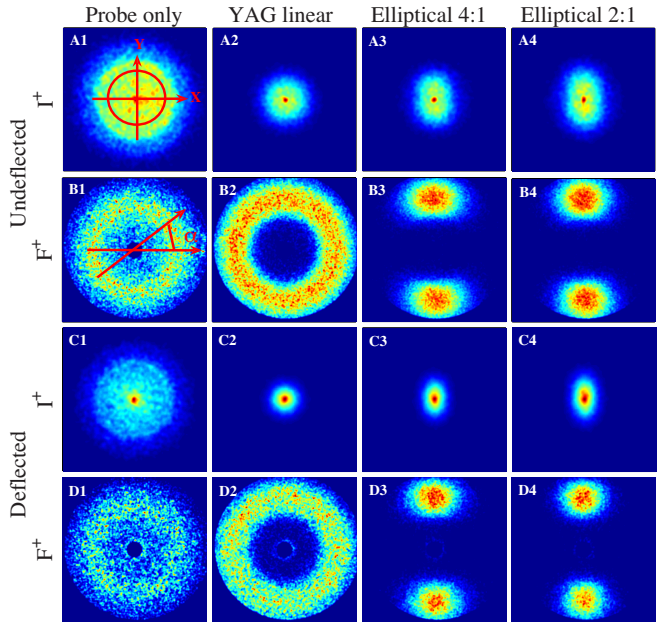

FIG. 4: (Color online) Ion images of I^+ and F^+ fragments recorded in end-view and at $I_{YAG,high}$ demonstrating 1D and 3D alignment. Columns: (1) probe only; (2) YAG linearly polarized; (3), (4) YAG elliptically polarized with an ellipticity intensity-ratio of 4:1 and 2:1, respectively. Rows: (A) I^+ images from undeflected molecules (0 kV); (B) F^+ images from undeflected molecules; (C) I^+ images from deflected molecules (10 kV); (D) F^+ images from deflected molecules.

applied to the deflector (Figure 4 C2).

The 1D alignment is also visible in the F^+ images. In the absence of the YAG pulse the F^+ image, recorded in the end-view, takes the form of a circularly symmetric ring (Figure 4 B1 and D1). This is caused by the fact that the linearly polarized probe field preferentially ionizes molecules with their C-I axis along its polarization vector [30]. When the linearly polarized YAG pulse is applied, the circular symmetry is conserved and the ring structure becomes more sharply defined to a localized radial area with no signal detected in the central region (Figure 4 B2 and D2). Such a ring structure is only compatible with the C-I axis being sharply aligned perpendicular to the detector plane and with the rotation of the molecular plane uniformly distributed around the C-I axis.

Next, we investigate the effect on the molecular alignment when the YAG polarization is changed from linear to elliptical. The end-view of the F^+ ions shows a dramatic change [Figure 4 B3, B4, D3, D4]. The initial circular symmetry is replaced by sharp localization along the minor axis (vertical in Figure 4) of the elliptically polarized YAG pulse. The angular localization of the F^+ ions, largest for the 2:1 ellipticity ratio (B4 and D4), shows that the molecular plane is confined to the plane defined by the elliptical polarization, and the conservation of their radial confinement shows that the C-I axis remains localized around the major polarization axis. To quantify the planar confinement the angular distributions of the F^+ ions were determined by radial integration of the images. The results are displayed in Figure 5. Focusing on panel (a), containing the undeflected data, it is seen that for the linearly polarized YAG pulse a uniform distribution emerges, whereas for elliptical polarization the angular distribution localizes. For the 4:1 ellipticity ratio (meaning that the intensity along the major axis is four times the intensity along the minor axis) the full widths at half maximum (FWHM) of the peaks in the angular distribution are 52.5°; for the 2:1 ratio they are 48.5°. Regarding the localization of the C-I axis, more precise insight is obtained by observing the I^+ end-view images. It is seen that the initial circular distribution (Figure 4 A2) develops into an elliptical shape when the YAG polarization is changed from linear to elliptical. This shows that the C-I axis has suffered a small distortion along the minor axis, remaining, however, tightly confined. The distortion is largest for the 2:1 ellipticity ratio. This is evident directly from the images as well as from the $\langle X \rangle$ and $\langle Y \rangle$ values. With the 4:1 ratio (A3) $\langle X \rangle = 18.1$ pixels and $\langle Y \rangle = 21.0$ pixels, whereas for the 2:1 ratio (A4) $\langle X \rangle = 18.2$ pixels and $\langle Y \rangle = 23.4$ pixels. Returning to the F^+ images the C-I axis distortion is actually visible by slightly more radial smearing in the 2:1 image compared to the 4:1 image. Thus, we conclude that the elliptically polarized YAG pulse induces pronounced 3D alignment of the DFIB. The confinement of the molecular plane increases as the polarization state is brought closer to circular polarization, but also gives rise to a larger distortion of the linear confinement of the C-I axis. These findings are consistent

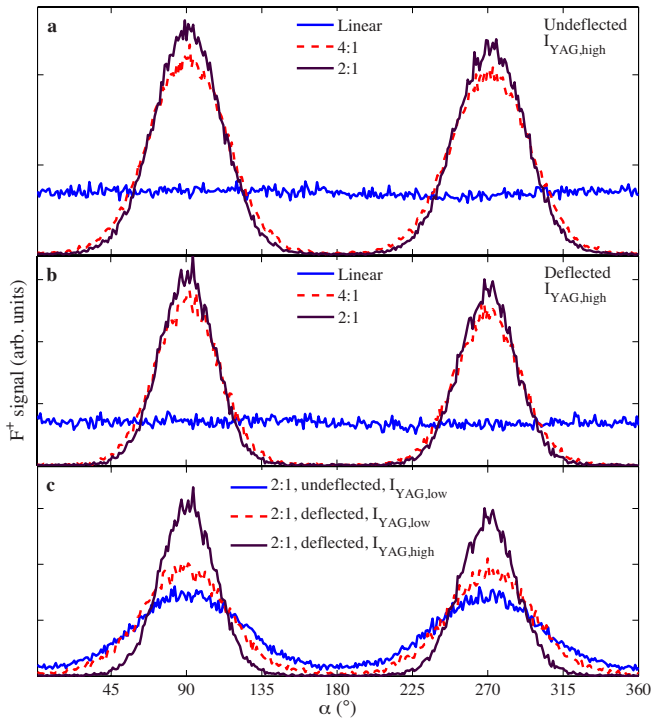

FIG. 5: (Color online) Angular distributions of the F^+ fragments for different YAG polarizations and intensities (α is pictorially defined in Figure 4 B1). (a) undeflected molecules under $I_{YAG,high}$ (b) deflected molecules under $I_{YAG,high}$; (c) comparison between the angular distributions with $I_{YAG,low}$ and $I_{YAG,high}$ for deflected molecules, where all the curves correspond to a 2:1 ellipticity ratio.

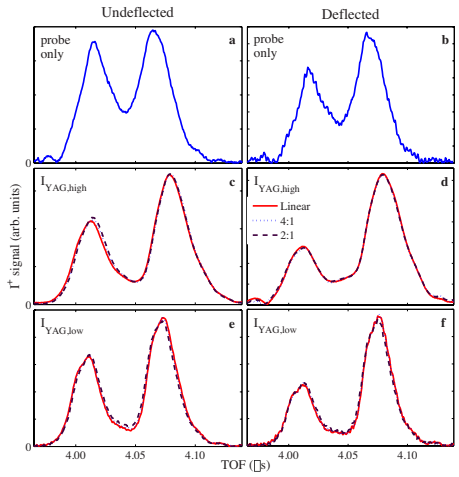

FIG. 6: (Color online) Time-of-flight spectra of the I^+ ions recorded under conditions of (a)–(b): probe pulse only; (c)–(d): high intensity YAG pulse ($I_{YAG,high}$); (e)–(f), (c)–(d): low intensity YAG pulse ($I_{YAG,high}$); In panel (c)–(f) the YAG polarization is linear (solid red curves), 4:1 elliptical (dotted blue curves), and 2:1 elliptical (dashed black curves). The data in the left column are recorded for undeflected and the data in the right column for deflected molecules.

with previous observations on other molecules [8, 9].

When the deflector is turned on the 3D alignment improves. The F^+ ion images show stronger confinement for both the 2:1 and the 4:1 configuration (Figure 4 D3, D4) compared to the corresponding undeflected data (Figure 4 B3, B4). This is also clear from the angular distributions in panel (b) of Figure 5. For the 4:1 ratio the FWHM decreases from 52.5° to 43.0°and for the 2:1 ratio from 48.5° to 37.0°. Turning to the I^+ end-view images in row C it is seen that although the C-I axis is still distorted when an elliptically YAG pulse is employed, the C-I axis confinement is much improved compared to the situation for undeflected molecules - compare Figure 4 C3, C4 to A3, A4. With the deflected molecules $\langle X \rangle$ = 10.7 pixels and $\langle Y \rangle$ = 15.3 pixels for the 4:1 ratio and $\langle X \rangle$ = 10.9 pixels and $\langle Y \rangle$ = 17.3 pixels for the 2:1 ratio. We conclude that both, 1D and 3D alignment, is significantly enhanced when using quantum-state selected molecules.

C. 1-dimensional and 3-dimensional orientation

Our final task is to prove that the molecules are oriented in addition to being aligned. This is accomplished by supplementing the ion images already presented by time of flight measurements of the I^+ ions. The most optimal information is obtained by using the end-view geometry. In this situation, the C-I axis is aligned parallel to the static electric field from the electrodes (693 V/cm) in the ion spectrometer. The TOF spectra of the I^+ ions will now allow us to conclude that the permanent dipole moment (directed from the carbon atom on the C_2 axis to the I atom) is preferentially pointing towards the repeller plate (high electrostatic potential) as we expect.

The TOF spectra recorded with the probe pulse alone are shown in Figure 6 (a) and (b). As mentioned in connection with the F^+ ion images the linearly polarized pulse is preferentially ionizing molecules with their axis along its polarization axis which explains the appearance of a forward and a backward peak [31] centered around at 4.045 μs. A mild asymmetry in the signal strength of the forward and the backward peak is observed. For undeflected molecules the asymmetry, defined as I_b^+/I_f^+ is 52/48. For the deflected molecules the asymmetry increases to 59/41.

To get an insight into the origin of this asymmetry we calculate the molecular orientation due to the static electric field itself. First, the ensemble-averaged orientation cosine $\langle \cos\theta \rangle$ is calculated quantum mechanically, where θ is the polar angle between the molecular C-I axis and the static field direction. For an ensemble at a rotational temperature of 1 K $\langle \cos\theta \rangle$ = 0.011, whereas for an ensemble corresponding to the state-selected molecules after the deflector (*height* = 1.2 mm, see Figure 2) $\langle \cos\theta \rangle$ = 0.079 [37]. To obtain the backward-forward ratio, b/f, we approximate the orien-

tational distribution function [32] by the truncated series $n(\theta) = 1 + a_1 \cdot P_1(\cos\theta) = 1 + 3 \cdot \langle\cos\theta\rangle \cdot \cos\theta$. Higher order Legendre polynomials can be neglected for the low electric field strength employed here. Furthermore, we assume that the molecules are probed with a detection efficiency scaling as $\cos^2\theta$ to account for the alignment selectivity of the probe pulse. Using the calculated values for $\langle\cos\theta\rangle$ we get $b/f = 52/48$ for the 1 K ensemble and $b/f = 60/40$ for the state-selected ensemble. Both numbers agree well with the observations. We conclude that the observed backward forward asymmetry in the time of flight spectra observed in the absence of the YAG pulse is due to weak orientation induced by the static field, as well as due to alignment selectivity of the probe beam.

When the YAG pulse is included two changes of the TOF spectra occur. First the forward and the backward peaks become more separated. This results from the strong alignment induced by the YAG pulse. All molecules are confined near the TOF axis, which will cause I^+ ions to be ejected directly towards or 180 degrees away from the detector, thus causing the maximum separation between the forward peaks. Second, the asymmetry increases. For the undeflected data (Figure 6 c) the backward-forward ratio is 63/37 and for the deflected data (Figure 6 d) 73/27. The TOF spectra for the elliptically polarized YAG (both 4:1 and 2:1 ratio) are essentially identical to the ones for the linearly polarized YAG. Therefore, we conclude that both strong 1D and strong 3D orientation are achieved. The degree of alignment, as well as the degree of orientation, improves considerably when the deflected molecules are employed.

D. Alignment and orientation at low laser intensity

There are many applications that would benefit strongly from being conducted on samples of 3D oriented molecules, e. g., photoelectron-angular-distribution measurements or diffractive imaging. Some of these applications may, however, also be negatively influenced, by the (moderately) intense field from the YAG pulse - in the worst case a certain application may not be possible at all when performed in the presence of the intense YAG field. The ideal situation is to obtain the 3D orientation under field-free conditions. This may be possible by, for instance, using timed perpendicularly polarized short pulses [13] or by turning off the long YAG pulse rapidly compared to the inherent molecular rotation times. In the case of 1D alignment and orientation it has been shown that such a conversion from adiabatic alignment/orientation to field-free alignment/orientation is possible by femtosecond truncation of the YAG pulse [33–35]. One consequence of the rapid turn-off method, or of other short pulse nonadiabatic alignment or orientation methods [36], is that the alignment/orientation becomes transient, which could reduce the utility for several important applications.

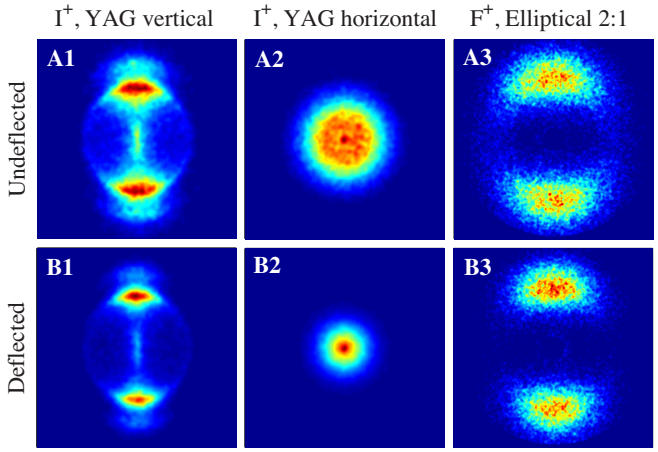

FIG. 7: (Color online) Ion images of I^+ and F^+ fragments recorded under $I_{YAG,low}$. Columns: (1) I^+ side-view; (2) I^+ end-view; (3) F^+, ellipticity ratio of 2:1. Rows: (A) undeflected molecules; (B) deflected molecules.

In the present work, we decided to test if strong 3D alignment and orientation could be maintained as the intensity of the YAG pulse was lowered, since a weaker alignment field also would reduce its influence in future applications. The ion images obtained at low YAG intensities, shown in Figure 7, reveal the same tendency as the high intensity images shown in Figure 4. They show considerably stronger confinement of the C-I axis and of the molecular plane, i. e., better 1D and 3D alignment, for deflected molecules relative to the undeflected molecules. In detail, the side-view image of the I^+ ions from the deflected molecules (Figure 7 B1) correspond to a value of $\langle\cos^2\theta_{2D}\rangle = 0.922$, and its end-view image (Figure 7 B2) shows a circular spot with $\langle X\rangle = 15.7$, and $\langle Y\rangle = 15.8$, whereas for the undeflected molecules $\langle\cos^2\theta_{2D}\rangle = 0.874$ (Figure 7 (A1)), and $\langle X\rangle = 22.5$, and $\langle Y\rangle = 22.6$ (Figure 7 A2).

The images of the F^+ ions (for a 2:1 ratio) exhibits stronger angular confinement when deflected molecules (Figure 7 C2) rather than undeflected molecules (Figure 7 C1) are used. This is also evident in the corresponding angular distributions in Figure 5 (c) that show a peak with a FWHM of 55.5° for the deflected molecules relative to more than 72° for the undeflected molecules. Finally, the TOF spectra, which indicate the degree of orientation, show a backward-forward asymmetry of 58/42 (Figure 6 e) for the undeflected molecules, which increases to 67/33 (Figure 6 f) for the deflected molecules. In summary, even when the intensity of the YAG alignment pulse is lowered by an order of magnitude a strong degree of 3D alignment and orientation is maintained, in accordance with previous findings for 1D alignment and orientation [21, 23].

IV. CONCLUSION

It was shown experimentally that 1-dimensional and 3-dimensional alignment and orientation of an asymmetric top molecule is significantly improved by selecting those molecules in a cold molecular beam that reside in the lowest rotational states. Alignment was induced in the adiabatic regime, where the turn-on and turn-off time of the linearly (1D alignment) or elliptically (3D alignment) polarized laser field occur slowly compared to the inherent rotational periods of the molecules. In addition, orientation, induced by the combined action of the laser field and a weak static electric field, is taking place in the adiabatic regime.

The alignment and orientation were illustrated by studies on 2,6-difluoroiodobenzene. Here, the major polarizability axis is parallel to the direction of the permanent dipole moment. Consequently, 3D orientation was achieved by positioning the major polarization axis of the elliptically polarized laser pulse along the direction of the static electric field. The case of the permanent dipole moment being parallel to the major polarizability axis occurs for a large number of molecules, and we expect that the method will be generally applicable for that case. Another possibility is that the major polarizability axis is perpendicular to the dipole moment. We believe that the elliptically polarized pulse should be sent such that the minor polarization axis coincides with the direction of the static electric field.

Finally, in the most general case, occurring for the largest range of molecules, the major polarizability axis and the permanent dipole moment differ by an angle that is neither zero nor ninety degrees. Achieving 3D orientation for this class of molecules attracts special interest since examples include important biomolecules such as amino acids and nucleic acids. We believe that 3D orientation can be achieved by turning the molecule, by rotating the axes of the elliptically polarized laser pulse, such that the permanent dipole moment coincides with the static field direction.

Acknowledgments

We thank Mikael P. Johansson for calculating the polarizability tensor of DFIB. Iftach Nevo acknowledges support from the Marie Curie IntraEuoropean Fellowships Network FP6. We also acknowledge support from the Carlsberg Foundation, the Lundbeck foundation, the Danish Natural Science Research Council, and the Deutsche Forschungsgemeinschaft within the priority program 1116.

[1] P. R. Brooks, Science **193**, 11 (1976).
[2] H. J. Loesch (editor), J. Phys. Chem. A **101** (1997), special issue on stereodynamics of chemical reactions.
[3] D. Herschbach, Eur. Phys. J. D **38**, 3 (2006).
[4] J. Itatani, J. Levesque, D. Zeidler, H. Niikura, H. Pépin, J. C. Kieffer, P. B. Corkum, and D. M. Villeneuve, Nature **432**, 867 (2004).
[5] V. Kumarappan, L. Holmegaard, C. Martiny, C. B. Madsen, T. K. Kjeldsen, S. S. Viftrup, L. B. Madsen, and H. Stapelfeldt, Phys. Rev. Lett. **100**, 093006 (2008).
[6] C. Z. Bisgaard, O. J. Clarkin, G. Wu, A. M. D. Lee, O. Gessner, C. C. Hayden, and A. Stolow, Science **323**, 1464 (2009).
[7] H. Stapelfeldt and T. Seideman, Rev. Mod. Phys. **75**, 543 (2003).
[8] J. J. Larsen, K. Hald, N. Bjerre, H. Stapelfeldt, and T. Seideman, Phys. Rev. Lett. **85**, 2470 (2000).
[9] S. S. Viftrup, Ph.D. thesis, Department of Physics and Astronomy, University of Aarhus (2007).
[10] H. Tanji, S. Minemoto, and H. Sakai, Phys. Rev. A **72**, 063401 (2005).
[11] A. Rouzee, S. Guerin, O. Faucher, and B. Lavorel, Phys. Rev. A **77**, 043412 (2008).
[12] J. G. Underwood, B. J. Sussman, and A. Stolow, Phys. Rev. Lett. **94**, 143002 (2005).
[13] K. F. Lee, D. M. Villeneuve, P. B. Corkum, A. Stolow, and J. G. Underwood, Phys. Rev. Lett. **97**, 173001 (2006).
[14] S. Viftrup, V. Kumarappan, S. Trippel, H. Stapelfeldt, E. Hamilton, and T. Seideman, Phys. Rev. Lett. **99**, 143602 (2007).
[15] S. Viftrup, V. Kumarappan, L. Holmegaard, C. Z. Bisgaard, H. Stapelfeldt, M. Artamonov, E. Hamilton, and T. Seideman, Phys. Rev. A **79**, 023404 (2009).
[16] B. Friedrich and D. Herschbach, J. Chem. Phys. **111**, 6157 (1999).
[17] B. Friedrich and D. Herschbach, J. Phys. Chem. A **103**, 10280 (1999).
[18] R. Baumfalk, N. H. Nahler, and U. Buck, J. Chem. Phys. **114**, 4755 (2001).
[19] H. Sakai, S. Minemoto, H. Nanjo, H. Tanji, and T. Suzuki, Phys. Rev. Lett. **90**, 083001 (2003).
[20] U. Buck and M. Farnik, Int. Rev. Phys. Chem. **25**, 583 (2006).
[21] L. Holmegaard, J. H. Nielsen, I. Nevo, H. Stapelfeldt, F. Filsinger, J. Küpper, and G. Meijer, Phys. Rev. Lett. **102**, 023001 (2009).
[22] V. Kumarappan, C. Z. Bisgaard, S. S. Viftrup, L. Holmegaard, and H. Stapelfeldt, J. Chem. Phys. **125**, 194309 (2006).
[23] F. Filsinger, J. Küpper, G. Meijer, L. Holmegaard, J. H. Nielsen, I. Nevo, and H. Stapelfeldt, J. Chem. Phys. **131** (2009), accepted, DOI: 10.1063/1.3194287.
[24] A. D. Becke, J. Chem. Phys. **98**, 5648 (1993).
[25] C. Lee, W. Yang, and R. G. Parr, Phys. Rev. B **37**, 785 (1988).
[26] A. Schäfer, C. Huber, and R. Ahlrichs, J. Chem. Phys. **100**, 5829 (1994).
[27] R. Ahlrichs, M. Bär, M. Häser, H. Horn, and C. Kölmel, Chem. Phys. Lett. **162**, 165 (1989).
[28] M. Hillenkamp, S. Keinan, and U. Even, J. Chem. Phys. **118**, 8699 (2003).
[29] N. F. Ramsey, *Molecular Beams* (Oxford University Press, 1956).
[30] J. J. Larsen, H. Sakai, C. P. Safvan, I. Wendt-Larsen, and

H. Stapelfeldt, J. Chem. Phys. **111**, 7774 (1999).
[31] P. Dietrich, D. T. Strickland, M. Laberge, and P. B. Corkum, Phys. Rev. A **47**, 2305 (1993).
[32] B. Friedrich, D. P. Pullman, and D. Herschbach, J. Phys. Chem. **95**, 8118 (1991).
[33] J. G. Underwood, M. Spanner, M. Yu Ivanov, J. Mottershead, B. J. Sussman, and A. Stolow, Phys. Rev. Lett. **90**, 223001 (2003).
[34] B. Sussman, J. Underwood, R. Lausten, M. Ivanov, and A. Stolow, Phys. Rev. A **73**, 053403 (2006).
[35] A. Goban, S. Minemoto, and H. Sakai, Phys. Rev. Lett **101**, 013001 (2008).
[36] O. Ghafur, A. Rouzee, A. Gijsbertsen, W. K. Siu, S. Stolte, and M. J. J. Vrakking, Nat. Phys **5**, 289 (2009).
[37] Since we have not performed a full simulation of the deflection profiles, as is described in reference 23, we have used the populations at the appropriate relative intensity value from the simulations on iodobenzene presented there.